WELDING RESEARCH

SUPPLEMENT TO THE *WELDING JOURNAL*, JANUARY 1993
Sponsored by the American Welding Society and the Welding Research Council

Toward Understanding Alloying Element Vaporization during Laser Beam Welding of Stainless Steel

A comprehensive model is proposed to predict vaporization rates during welding. Predictions are compared with experimental data

BY K. MUNDRA AND T. DEBROY

ABSTRACT. During laser beam welding of many important engineering alloys, appreciable changes in the composition and properties of the weld metal can occur due to pronounced vaporization of alloying elements from the weld pool. Currently there is no comprehensive theoretical model to predict, from fundamental principles, laser-induced metal vaporization rates and the resulting weld pool composition changes.

The velocity distribution functions of the gas molecules at various locations above the weld pool surface and the heat transfer and fluid flow phenomena in the pool have been coupled to model the rates of the vaporization of various alloying elements during laser beam welding of stainless steels. The procedure allows for computation of both the evaporation and condensation fluxes based on the equations of conservation of mass, momentum and energy applied to the vapor and the liquid phases. Computed values of the rates of vaporization of various alloying elements and the vapor composition were found to be in good agreement with the corresponding experimental values. Synthesis of the principles of gas dynamics and weld pool transport phenomena can serve as a basis for the calculation of alloying element vaporization rates during laser beam welding of alloys.

K. MUNDRA and T. DEBROY are with the Department of Materials Science and Engineering, Pennsylvania State University, University Park, Pa.

Introduction

The use of a high power density laser beam for welding leads to weld pool temperatures that are often higher than those encountered in most other welding processes. Even at modest power densities, laser beam welding of many important engineering alloys results in significant changes in composition and properties of the weld metal (Refs. 1–4). Because of its importance, vaporization of alloying elements during welding has been investigated both experimentally and theoretically. Apart from the examination of the weld metal composition and structure to evaluate the direct effects of vaporization, much of the previous experimental work was based on in-situ monitoring of the alloying element vaporization by emission spectroscopy (Refs. 5–7). It was found that during welding of stainless steels, the dominant species in the vapor phase were iron, manganese, nickel and chromium. Eagar and Block-Bolton (Ref. 8) used calculations based on the Langmuir equation to demonstrate that iron and manganese were the most prominent vapor species in the welding environment. Although the rates calculated by the Langmuir equation have been used for the determination of the relative vaporization rates of various alloying elements, the calculated vaporization rates are generally significantly higher than the corresponding experimentally determined values at one atmosphere pressure. Even at pressures as low as 200 micrometers of Hg, the vaporization rates of pure

KEY WORDS

Modeling
Vaporization Rates
Alloying Elements
Laser Beam Welding
Gas Dynamics
Weld Pool Transport
Evaporation Heat Loss
Peak Temperatures
Vapor Composition
Shielding Gas

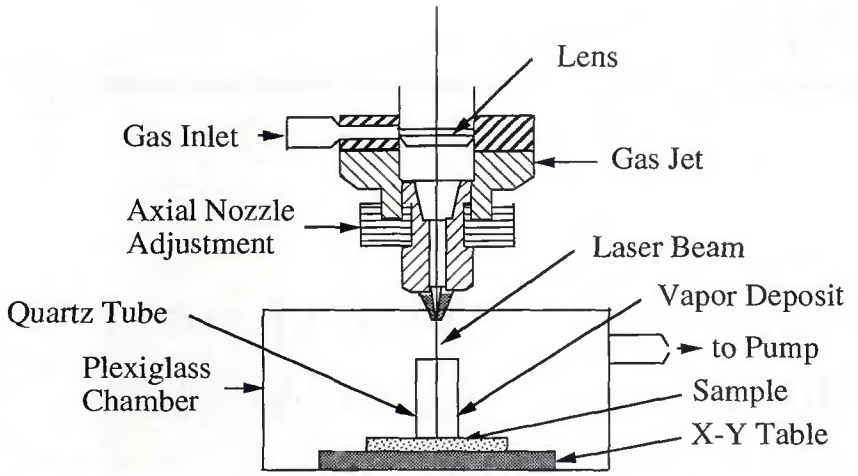

Fig. 1 — A schematic diagram of the experimental setup.

metal drops were found (Ref. 9) to be about an order of magnitude lower than the values calculated by the Langmuir equation.

When a metal is irradiated with a very high power density laser beam, a significant amount of vapor condensation can take place and the kinetics of condensation must be taken into account in the calculation of the net vaporization rate. Anisimov (Ref. 10) calculated the vapor condensation rate by solving the gas dynamics equations in a thin layer adjacent to liquid metal-vapor interface, known as the Knudsen layer. However, the calculations of temperature at the metal surface were done from an approximate energy balance which included only the energy required for the vaporization, and completely ignored heat transfer due to conduction and convection. For vaporization of aluminum, Knight (Ref. 11) derived a set of gas dynamic equations across the Knudsen layer and calculated the fraction of the vaporized material that condenses for a given local surface temperature. Recently, Chan and Majumdar (Ref. 12) used Knight's equations to calculate laser-induced material vaporization rates from molten aluminum, titanium and a superalloy. In the works of Knight (Ref. 11) or Chan and Majumder (Ref. 12), the temperature calculations were performed in one dimension. Furthermore, no comparison between the theoretical predictions and the experimental results was undertaken for the irradiation of either pure metals or alloys.

Since Anisimov's work (Ref. 10), significant progress has been made in the application of transport phenomena for the calculation of weld pool temperature and velocity fields. At present, weld pool temperature calculations are commonly performed by taking into account both heat conduction and Marangoni convection in the weld pool. DebRoy, Basu and Mundra (Ref. 13) combined the principles of weld pool transport phenomena and the vapor phase gas dynamics for the calculation of laser-induced vaporization of pure metals. The computed results agreed well with the experimental data for the vaporization of iron and titanium. The agreement between the experimental and theoretical results for pure metals indicates promise of such a comprehensive calculation scheme in realistic modeling of the rates of vaporization of alloying elements during laser beam welding of alloys.

The work reported in this paper is aimed at understanding laser-induced vaporization of stainless steels. The fluid flow and temperature fields in the molten pool were simulated by the solution of the Navier-Stokes equations and equation of conservation of energy. The heat transfer to the shielding gas and the evaporative heat loss (Ref. 14) due to vaporization of the alloying elements were taken into account in the calculations. The computed weld pool temperature distribution was used together with the principles of gas dynamics and mass transfer for the calculation of the vaporization rates during laser beam welding of AISI 202 stainless steel in the continuous wave mode. The rates of vaporization of alloying elements due to a total pressure gradient at the pool surface were determined from the equations of conservation of mass, momentum and translational kinetic energy in the gas phase. In addition, mass transfer rates due to concentration gradients were determined using available correlations amongst various dimensionless numbers. The theoretically predicted rates of vaporization of iron, manganese, nickel and chromium from a molten AISI 202 stainless steel weld pool were compared with the corresponding experimentally determined values. Furthermore, the effects of the nature and the flow rate of the shielding gas on the vaporization rate were examined on the basis of the model.

Experimental Procedure

The details of the experimental procedure are given in Refs. 2 and 15 from where the experimental data were taken for the validation of the model. A continuous wave carbon dioxide laser was used to irradiate samples of AISI 202 steel as shown in Fig. 1. The total rate of vaporization was determined from the loss in sample weight and the laser material interaction time. A portion of the vaporized material was collected as condensate on the inner surface of a hollow, cylindrical, open-ended quartz tube which was held stationary and coaxial with the laser beam. The rates of vaporization of the individual alloying elements were determined from the total vaporization rate and the composition of the condensate was analyzed by electron probe microanalysis (EPMA).

Theoretical Investigation

Temperature and Velocity Profiles in the Molten Pool

The rates of vaporization of the various alloying elements from the weld pool are strongly dependent on the temperature distribution at the pool surface. Direct reliable measurements of temperature profile at pool surface is difficult since the weld pool is small in size and is often covered by an intense plasma (Refs. 5–7) which interferes with most noncontact temperature measurement procedures. Procedures based on the selective vaporization of alloying elements (Ref. 2) do not provide spatial resolution of the temperature at the pool surface. A recourse is to simulate temperature fields by mathematical modeling of the essential physical features of the process. The task involves numerical solution of the Navier-Stokes equation and the equation of conservation of energy. This approach has been adopted in this paper. Since the appropriate equations are well documented in standard textbooks, and the boundary conditions and other details of the application of these equations to welding are available in the recent welding literature (Refs. 16–18), these are not presented here. Special features of the computational scheme that have been taken into account in the boundary conditions include the heat transfer to the shielding gas from the surface of the pool and the evaporative heat loss due to vaporization of alloying elements. Zacharia, *et al.* (Ref. 14), has

shown that vaporization can significantly influence the temperature field on the pool surface. The local heat flux from the pool surface, J_h, in J/m^2-s is given by

$$J_h = h\{T_1 - T_g\} + \sum_{i=1}^{n} J_i \Delta H_i \qquad (1)$$

where T_1 is the local weld pool surface temperature, T_g is the ambient temperature, J_i is the vaporization flux in kg/m^2-s of an element i, ΔH_i is the enthalpy of vaporization of the element i in J/kg, n is the number of alloying elements and h is the heat transfer coefficient in J/m^2-s-K. The heat transfer coefficient for a gas jet impinging on a surface was derived from the graphical results of Schlunder and Gniclinski (Ref. 19) and is given by the following relation:

$$h = \frac{2Pr^{0.42}\,Re^{0.5}\,k}{d}\left(1+\frac{Re^{0.55}}{200}\right)^{0.5} \left[0.483 - 0.108\frac{r}{d} + 7.71\times10^{-3}\left\{\frac{r}{d}\right\}^2\right] \qquad (2)$$

where d is the diameter of the nozzle in meters, r is the radial distance on the pool surface in meters, k is the thermal conductivity of shielding gas in J/m-s-K at temperature T_{av}, which is the arithmetic average of T_1 and T_g, Re is the Reynolds number at the nozzle exit and Pr is the Prandtl number.

Vaporization Due to Pressure Gradient

In laser processing of the metals and alloys, the temperatures reached on the surface can be very high and often exceed the boiling point (Refs. 20, 21). For example, von Allmen (Ref. 22) determined molten pool temperatures in excess of boiling point for laser treatment of copper. Batanov, *et al.* (Ref. 23), indicated that temperatures on the surface of the laser irradiated material can be higher than the normal boiling point of the material. Paul and DebRoy (Ref. 16) and Zacharia, *et al.* (Ref. 24), have reported temperatures close to the boiling point for laser beam welding. Khan and DebRoy (Ref. 2) measured the liquid pool surface temperatures close to the boiling point from the ratio of the rates of vaporization of alloying elements. Chan and Majumdar (Ref. 12) have also reported temperatures greater than boiling point for the laser irradiation of aluminum, titanium and a superalloy. Theoretical calculations of the vaporization rates by Knight (Ref. 11) and Anisimov (Ref. 10) are based on the premise that the liquid pool surface temperatures are higher than the boiling point.

At temperatures higher than the boiling point, the pressures in the vicinity of the pool are greater than the ambient pressure and the excess pressure provides a driving force for the vapor to move away from the surface. The velocity distribution functions of the vapor molecules escaping from the weld pool surface at various locations are shown schematically in Fig. 2. Near the weld pool surface, the molecules cannot travel in the negative direction, and as a consequence, the distribution function is half-Maxwellian. Close to the weld pool surface there exists a space of several mean free paths length, known as the Knudsen layer (Ref. 10), at the outer edge of which the velocity distribution reaches the equilibrium distribution. Here, the vapor molecules can have all possible velocities from $-\infty$ to $+\infty$, at least in principle, as observed in Fig. 2. A portion of the vaporized material condenses on the liquid surface.

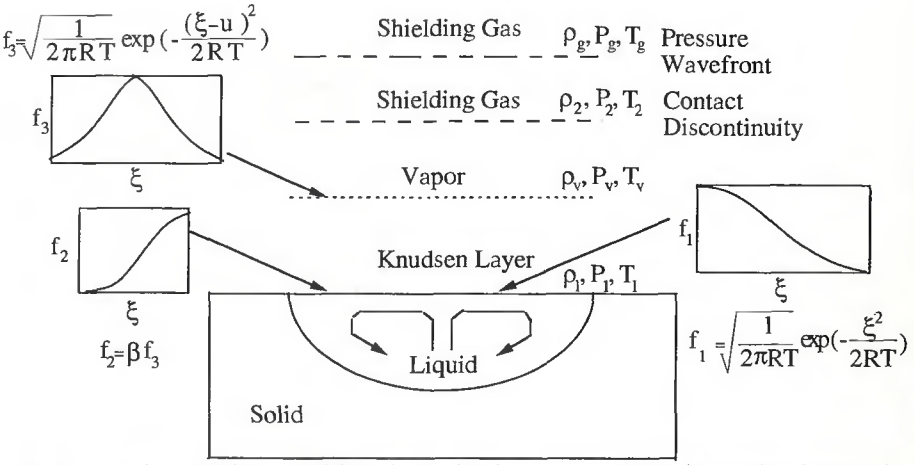

Fig. 2 — A schematic diagram of the velocity distribution junctions in the Knudsen layer and in adjacent regions.

The temperature T_v, density ρ_v, pressure P_v and the mean velocity of the vapor, u, at the edge of the Knudsen layer can be related to temperature, T_1, pressure, P_1, and the density, ρ_1, of the vapor at the liquid surface by treating the Knudsen layer as a gas-dynamic discontinuity. Anisimov (Ref. 10) and Knight (Ref. 11) derived expressions for the changes in the vapor density, temperature, velocity and the extent of condensation by using the velocity distribution functions presented in Fig. 2 and solving the equations of conservation of mass, momentum and translational kinetic energy across the Knudsen layer. Since the details of the procedure are available in their papers, only a summary of the results, commonly referred to as the jump conditions, are presented in Equations 3 to 5.

$$\frac{T_v}{T_1} = \left(\sqrt{1+\pi\left(\frac{\gamma_v-1}{\gamma_v+1}\frac{m}{2}\right)^2} - \sqrt{\pi}\,\frac{\gamma_v-1}{\gamma_v+1}\frac{m}{2}\right)^2 \qquad (3)$$

where $m = u/\sqrt{2\,R_v\,T_v}$, $R_v = R/M_v$, R is the gas constant in J/mole-K, γ_v is the ratio of specific heats of the vapor, which is treated as a monoatomic gas, and M_v is the average molecular weight of the vapor in kg/kg-mole

$$\frac{\rho_v}{\rho_1} = \sqrt{\frac{T_1}{T_v}}\left(\left(m^2+\frac{1}{2}\right)e^{m^2}\,erfc(m) - \frac{m}{\sqrt{\pi}}\right) + \frac{1}{2}\frac{T_1}{T_v}\left(1-\sqrt{\pi}\,m\,e^{m^2}\,erfc(m)\right) \qquad (4)$$

where erfc is the complimentary error function.

The condensation factor, β, is given by

$$\beta = \left(\left(2m^2+1\right) - m\sqrt{\pi\frac{T_1}{T_v}}\right)e^{m^2}\frac{\rho_1}{\rho_v}\sqrt{\frac{T_1}{T_v}} \qquad (5)$$

The density, ρ_1, can be computed from P_1 and T_1, assuming that the vapor behaves like an ideal gas. The equilibrium vapor pressure, P_1, at the pool surface is obtained from the equilibrium vapor pressure-temperature relationships of the various alloying elements.

$$\frac{P_1}{P_g} = \sum_{i=1}^{n} a_i \frac{P_i^\circ}{P_g} \qquad (6)$$

where P_g is the ambient pressure, a_i is the activity of the alloying element i and P_i° is the equilibrium vapor pressure of the pure element i at T_1 and n is the number of alloying elements. Since the temperatures at the weld pool surface are very high, the activities were taken to be equal to the corresponding mole fractions. The average molecular weight of the vapor, M_v, in the Knudsen layer is given by:

$$M_v = \sum_{i=1}^{n} M_i \frac{a_i P_i^\circ}{P_1} \qquad (7)$$

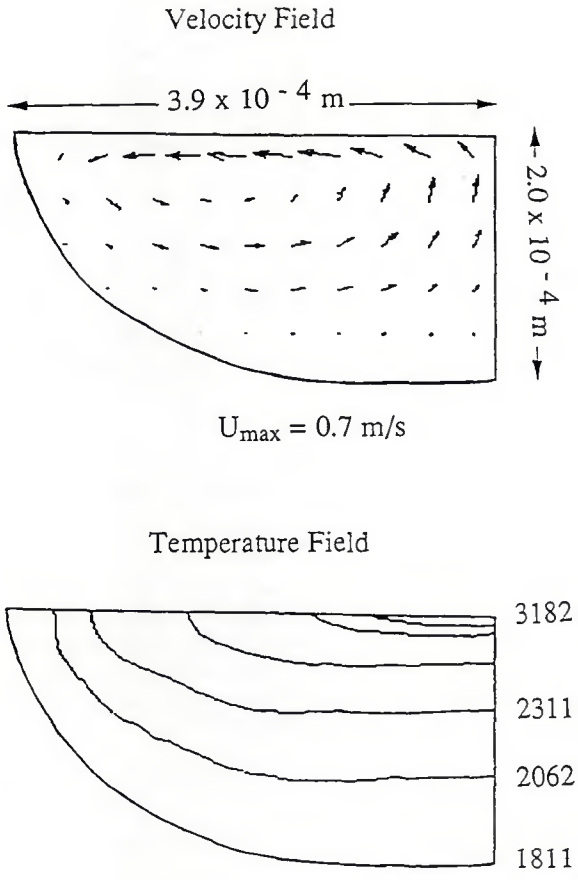

Fig. 3 — Velocity and temperature fields for a laser power of 560 W and helium gas flow rate of 6 L/min.

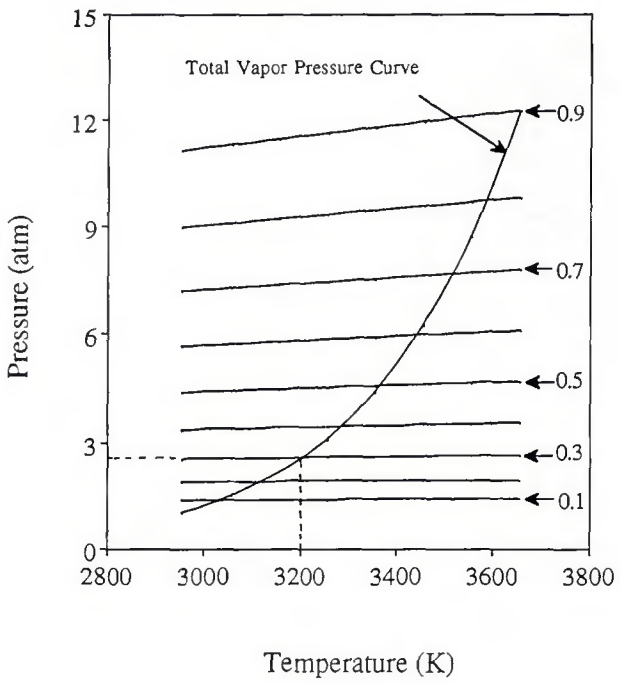

Fig. 4 — Flow state diagram for AISI 202 stainless steel in helium atmosphere. The Mach number for various lines is indicated in the figure.

where M_i is the molecular weight of species i, a_i is the activity i in the liquid metal, and P_i° is the equilibrium vapor pressure of the pure element i at T_1. Since there are four unknowns in Equations 3 to 5, *viz.* T_v, p_v, ß and m, it is necessary to have an additional equation to have unique values of these variables. The necessary equation is obtained by relating the pressure at the edge of the Knudsen layer to the ambient conditions. Across the Knudsen layer the vapor wavefront moves into the shielding gas, as shown in Fig. 2. The moving interface between the vapor and the shielding gas is a contact discontinuity. Across this discontinuity, the pressures are the same, *i.e.*, $P_2 = P_v$. The pressure rise at the liquid-vapor interface propagates as a pressure wave as shown in Fig. 2. The wavefront may be treated as a pressure discontinuity, and the pressure change across the wavefront may be obtained by applying the Rankine-Hugoniot relation (Ref. 25).

$$\frac{P_1}{P_g}\frac{P_2}{P_1} = 1+\gamma_g M\Gamma\left(\frac{\gamma_g+1}{4}M\Gamma+\sqrt{1+\left(\frac{\gamma_g+1}{4}M\Gamma\right)^2}\right) \quad (8)$$

where P_g and P_2 are the pressures in front of and behind the wavefront, respectively. γ_g is the ratio of specific heats for shielding gas and $\Gamma = \sqrt{\gamma_v R_v T_v}/\sqrt{\gamma_g R_g T_g}$. The Mach number, M, is related to m according to the equation

$$m = M\sqrt{\frac{\gamma_v}{2}} \quad (9)$$

In Equation 8, P_1/P_g can be computed from Equation 6 for a given local surface temperature and, since $P_2 = P_v$, for an ideal gas, P_2/P_1 can be expressed as a function of m with the help of Equations 3 and 4. Thus, Equation 8 is effectively reduced to a nonlinear equation in m and can be solved iteratively or graphically to obtain m and the Mach number for a given local weld pool surface temperature. The values of T_v, p_v and ß, corresponding to a local temperature T_1 can be determined from Equations 3 to 5 by using the computed value of m. The Mach number and the density ρ_v can then be used to calculate the vaporization flux, J_p, in kg/m^2-s, due to pressure gradient at the pool surface corresponding to a local surface temperature T_1.

$$J_p = \rho_v MS \quad (10)$$

where S is the speed of sound in vapor at temperature T_v. Since the rate of vaporization of an alloying element will be proportional to its partial pressure over the pool, its flux, J_{pi} is given by

$$J_{p,i} = a_i \frac{p_i^\circ}{P_1}\frac{M_i}{M_v}J_p \quad (11)$$

Vaporization Due to Concentration Gradient

At the pool surface, the concentrations of the alloying elements in the vapor is considerably higher than their respective concentrations in the bulk shielding gas. The vaporization flux of an element i due to concentration gradient, $J_{c,i}$ in kg/m^2-s, is then defined as

$$J_{c,i} = K_{g,i} M_i \frac{a_i P_i^\circ}{RT_1} \quad (12)$$

where P_i° is equilibrium vapor-pressure of the element i over pure liquid i in atmosphere, M_i is the molecular weight of the element i in kg/kg-mole, R is the gas constant in m^3 atm /kg-mole K and $K_{g,i}$ is the mass transfer coefficient of the element i in m/s. The mass transfer coefficient was derived form the graphical

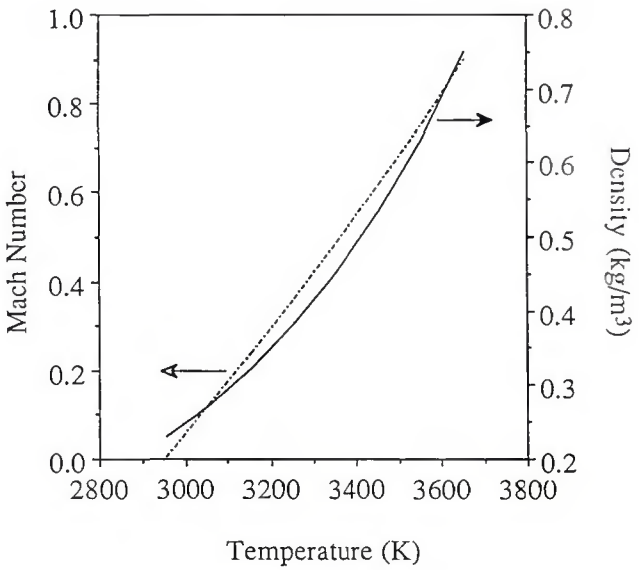

Fig. 5 — Mach number and density for AISI 202 stainless steel for various temperatures at the edge of Knudsen layer in helium atmosphere.

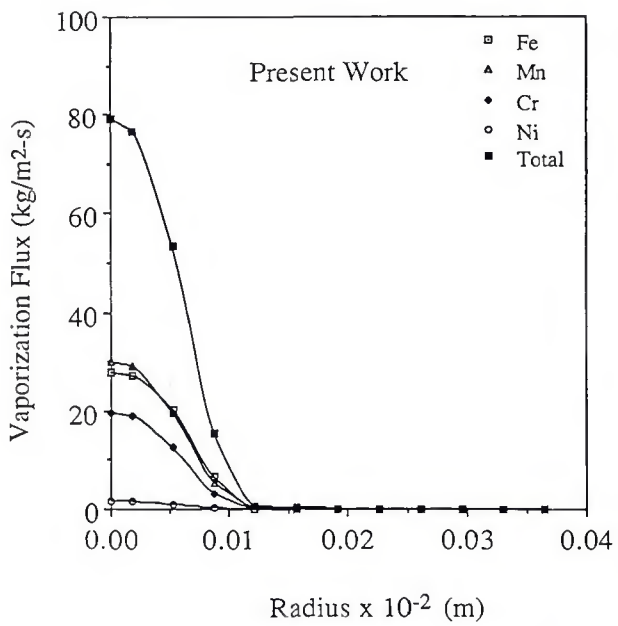

Fig. 6 — Vaporization flux for various alloying elements, and the total flux from the model presented in this paper.

results of Schlunder and Gniclinski (Ref. 19) and is given by

$$K_{g,i} = \frac{2Sc^{0.42}\,Re^{0.5}\,D}{d}\left(1+\frac{Re^{0.55}}{200}\right)^{0.5}\left[0.483-0.108\frac{r}{d}+7.71\times10^{-3}\left\{\frac{r}{d}\right\}^2\right] \qquad (13)$$

where d is the diameter of the nozzle in meters, r is the radial distance on the pool surface in meters, D is the diffusivity of the element in shielding gas in m^2/s at temperature T_{av}, Re is the Reynolds number at the nozzle exit and Sc is the Schmidt number of the element at average temperature T_{av}. The total vaporization flux, J_i, for an element i is then given by

$$J_i = J_{p,i} + J_{c,i} \qquad (14)$$

Results and Discussion

Velocity and Temperature Fields

When the laser beam strikes the surface of the samples, melting occurs almost instantaneously. For a high power density laser beam, the time required to reach steady state is very small. Zacharia, *et al.* (Ref. 24), noted that in laser beam welding quasi-steady state is achieved very quickly. Mehrabian, *et al.* (Ref. 26), showed that the time required to reach the maximum melt depth in iron for a laser power of 2×10^5 W/cm² is of the order of 1 ms. Thus, for almost the entire duration of a large laser pulse of several milliseconds span, the molten pool remains in a steady state. The

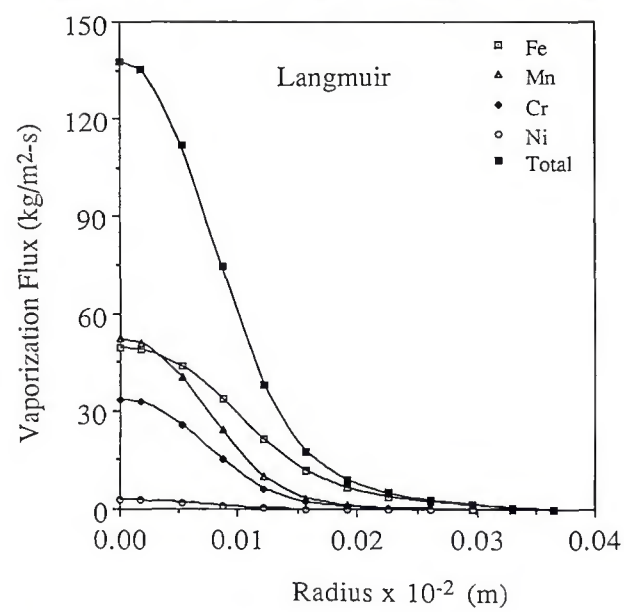

Fig. 7 — Vaporization flux for various alloying elements and the total flux computed using Langmuir equation.

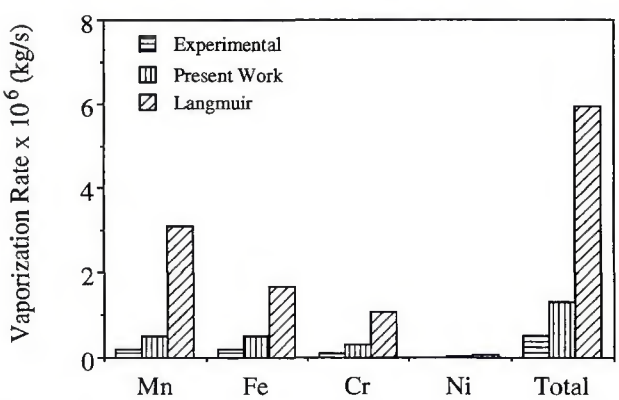

Fig. 8 — Comparison of the experimental vaporization rates with the rates calculated from the Langmuir equation and from the model presented in this paper.

Table 1 — Data Used for Calculations in the Welding of AISI 202 Stainless Steel

Property/Parameter	Value
Density (kg/m^3)	7200.0
Melting point (K)	1811.0
Laser power (W)	560.0
Radius of the beam (m)	2.0×10^{-4}
Effective viscosity (kg/m-s)	0.05
Thermal diffusivity of solid (m^2/s)	3.3×10^{-5}
Thermal diffusivity of liquid (m^2/s)	7.5×10^{-5}
Specific heat of solid (J/kg-K)	710.6
Specific heat of liquid (J/kg-K)	836.0
Absorption coefficient	0.17
Temperature coefficient of surface tension (N/m-K)	-5.3×10^{-4}
Ratio of specific heats of vapor (γ_v)	1.667

Table 2 — Enthalpies of Vaporization of the Alloying Elements[a]

Element	Enthalpy (kJ/kg)
Iron	6087
Manganese	4005
Chromium	6577
Nickel	6388

(a) Ref. 27.

Table 3 — Comparison of Predicted Values of Weld Pool Geometry and Peak Temperatures with Experimental Data for the Welding of AISI 202 Stainless Steel

Parameter	Experimental[a]	Model Prediction
Welding pool width (m)	8.2×10^{-4}	7.8×10^{-4}
Weld pool depth (m)	2.3×10^{-4}	2.0×10^{-4}
Peak temperatures (K)	3093 ± 44	3182

(a) Refs. 2, 15.

Table 4 — Composition of the Alloying Elements in the AISI 202 Stainless Steel

Elements	Composition (wt-%)	Activity (mole fraction)
Manganese	6.58	0.066
Chromium	17.80	0.190
Nickel	4.77	0.045
Iron	70.14	0.698

Table 5 — Comparison of the Predicted Vapor Composition with the Experimentally Determined Values for the Welding of AISI 202 Stainless Steel

Composition Ratio (Moles of i/ Moles of j)	Experimental	Present Work
J_{Fe}/J_{Mn}	1.08 ± 0.07	1.00
J_{Cr}/J_{Mn}	0.56 ± 0.08	0.65
J_{Ni}/J_{Mn}	0.05 ± 0.01	0.05

steady state temperature and velocity fields, obtained from the solution of Navier-Stokes equations and the equations of conservation of mass and energy are shown in Fig. 3. The calculation takes into consideration the convective heat loss to the shielding gas and the evaporative heat loss at the pool surface in accordance with Equation 1. The data used for the calculations are presented in Tables 1 and 2. The details of the calculations of thermal diffusivity and viscosity of the shielding gas are presented in Appendix B. For low concentration of surface active elements, the temperature coefficient of surface tension is negative (Ref. 29). Therefore, the velocities at the weld pool surface, shown in Fig. 3, are radially outward resulting in a relatively shallow pool. The maximum radial velocity is of the order of 0.7 m/s, which is close to the value reported by Zacharia, *et al.* (Ref. 24). The computed strong temperature gradient on the surface of the pool is consistent with the absorption of a significant amount of energy in a small localized area near the laser beam axis. The theoretically predicted pool diameter and depth, presented in Table 3, were found to be in good agreement with the experimentally observed values (Refs. 2, 15). Furthermore, the theoretically predicted peak temperature indicated in Table 3 was found to be in good agreement with the temperature experimen-

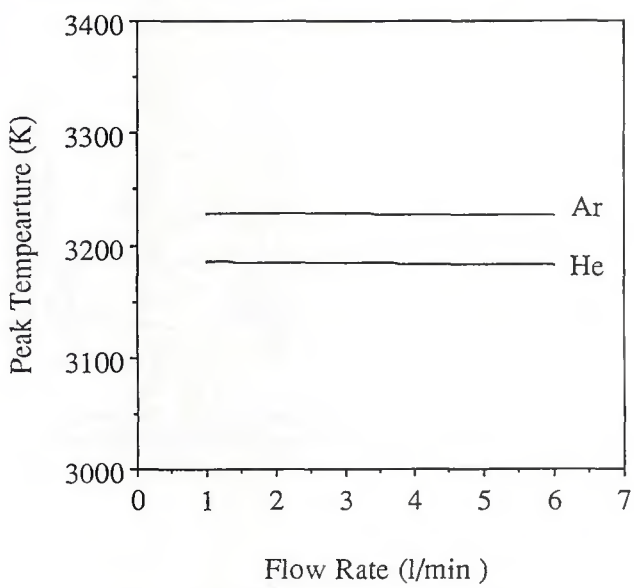

Fig. 9 — Peak temperatures calculated as a function of gas flow rate and the type of the shielding gas used.

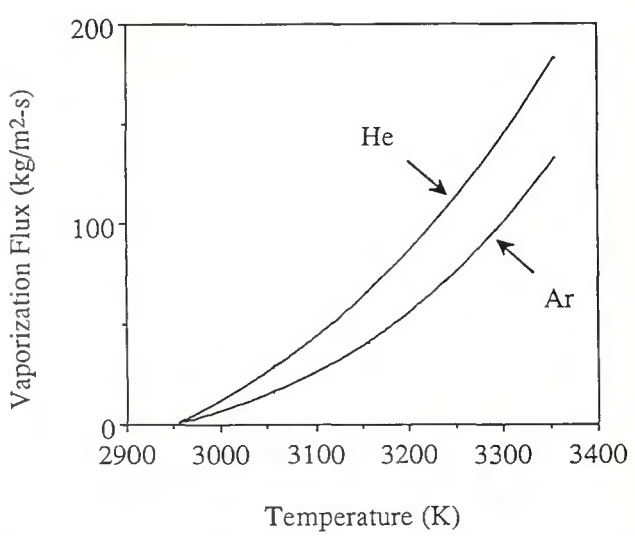

Fig. 10 — Pressure gradient driven vaporization flux as function of temperature in helium and argon.

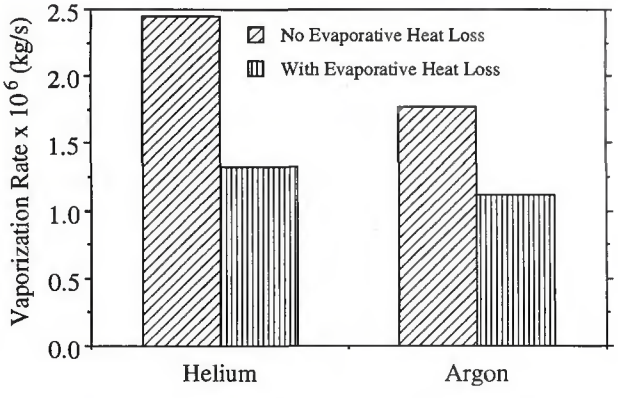

Fig. 11 — Comparison of vaporization rate in helium and argon for a flow rate of 6 L/min with or without consideration of evaporative heat loss.

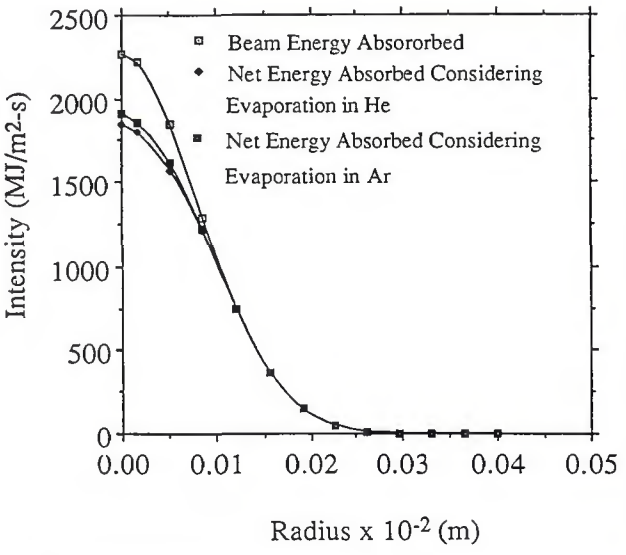

Fig. 12 — Energy absorbed vs. radius.

tally determined by Khan and DebRoy (Ref. 2).

The computed results demonstrate the importance of weld pool evaporative heat flux in the calculation of the peak temperature. For a gas flow rate of 6 L/min of helium, the peak temperature was found to be 3222 K when the evaporative heat loss was not considered whereas when the heat loss was considered, the peak temperature dropped to 3182 K. These results are consistent with the observations of Zacharia, *et al.* (Ref. 14), who reported a significant drop in the temperature when evaporative heat loss from the pool surface was considered.

Vaporization Rates

From the temperature field in Fig. 3, it is evident that the temperatures reached at the weld pool surface are high and the temperature at the center of the pool is greater than the boiling point of pure iron. The temperature at which the pressure on the surface is equal to 1 atm was calculated to be 2952 K from the equilibrium vapor pressure-temperature relationship for the various alloying elements given in Appendix C and the composition of the AISI 202 stainless steel indicated in Table 4. When the local surface temperature is higher than this value, the pressure at the weld pool surface is greater than the ambient pressure. In such a case, the relations among the temperature, pressure and the Mach number for a material can be represented on a plot of temperature vs. pressure for various values of Mach number. The plot, commonly referred to as the flow state diagram, obtained from the solution of Equations 3 to 9, is shown in Fig. 4. The Mach number of the vapor across the Knudsen layer is uniquely defined and is given by the Mach number of the line that intersects the equilibrium vapor pressure curve at a given temperature. For example, the Mach number of the vapor across the Kundsen layer at weld pool surface temperature of 3200 K is 0.3 and the equilibrium vapor pressure at the pool surface is 2.5 atm. The values of the Mach number and the density of the vapor across the Knudsen layer calculated from Equation 4 for various surface temperatures are presented in Fig. 5. The computed values of both the Mach number and the vapor density indicate their strong dependence on the surface temperature due mainly to the strong correlation between the vapor pressure and temperature. From the values of the Mach number and the density, total vaporization flux and the flux of the individual alloying elements due to pressure gradient are calculated from Equations 10 and 11. The vaporization rate due to concentration gradient is calculated from mass transport considerations, which take into account the gas flow conditions and the nature of the shielding gas in accordance with Equation 12.

The radial distribution of the vaporization flux of the alloying elements and the total flux due to the combined effects of total pressure and concentration gradients are plotted in Fig. 6. Similarly, the radial distribution of the vaporization flux of the individual alloying elements and the total flux calculated from the Langmuir equation are plotted in Fig. 7. Comparison of the results in Figs. 6 and 7 indicates that the flux of the alloying elements predicted from the Langmuir equation is much higher than the corresponding value predicted from the present work. In Fig. 8, the experimentally determined vaporization rates for the AISI 202 stainless steel are compared with the rates computed from the model and the values calculated from the Langmuir equation for the same steel. It is observed that the experimentally determined vaporization rates are closer to the values predicted by the present model than the rates calculated from the Langmuir equation. Furthermore, the predicted ratios of the vaporization rates of the alloying elements are in good agreement with the corresponding experimentally determined values as observed from Table 5.

The effects of the nature and the flow rate of the shielding gas on the weld pool temperature are observed from the results in Fig. 9 where the calculated peak temperatures in helium and argon are indicated. The observed temperature difference in the two cases is about 35 K. At a peak temperature of about 3200 K, this difference would be difficult to determine experimentally. For a given shielding gas, the calculations indicate that with the increase in the gas flow rate, the peak temperature on the pool surface does not change significantly as can be observed from Fig. 9.

To understand the effect of the type of shielding gas, let us consider isothermal evaporation in helium and argon driven by the pressure gradient alone, since the pressure gradient driven mass transfer rate is significantly higher than the concentration gradient driven rate. In such a case, at a given temperature, the computed results in Fig. 10 indicate a higher vaporization rate in helium than that in argon. This is due to the fact that condensation of vapor molecules is more pronounced in argon than in helium due to the differences in the physical properties of the two gases, particu-

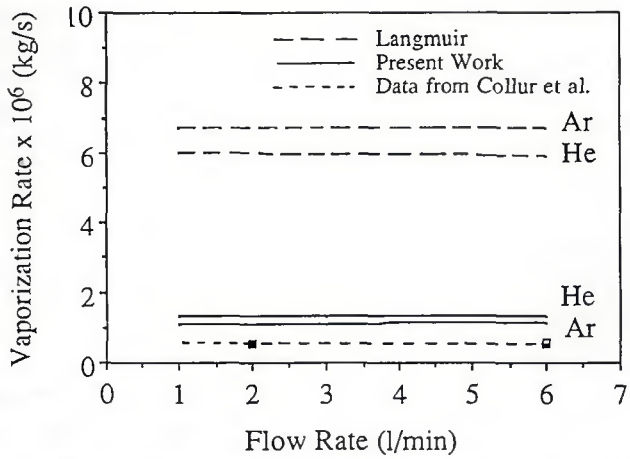

Fig. 13 — Vaporization rate predicted from the model and from the Langmuir equation for different types of shielding gas at various flow rates. Experimental vaporization rates are taken from Ref. 4.

larly the densities. The connective heat loss to the shielding gas is considerably smaller than the laser beam energy absorbed by the weld pool. Therefore, if the evaporative cooling were ignored and the computed weld pool surface temperature distributions were identical in helium and in argon, the computed vaporization rates in helium would have been much higher in helium than that in argon, as can be observed from Fig. 11. In the absence of evaporative heat loss, the radial distribution of the net energy absorption is shown by the uppermost curve in Fig. 12. However, when the evaporative heat loss is considered, the net absorbed energy in argon atmosphere is slightly higher than that in helium, as can be observed in Fig. 12. The difference in the net energy absorption in argon and helium results in about 35 K lower peak temperature in helium atmosphere as has been discussed earlier. The lower temperature in helium compensates the difference in vaporization rates when evaporative heat loss is considered. The resulting vaporization rate is about 15% higher in helium than in argon. The calculated results are consistent with the observations of Collur, *et al.* (Ref. 4), who measured vaporization rates during laser beam welding of AISI 201 stainless steel in different shielding gases at various shielding gas flow rates. He found that the vaporization rate did not change significantly with either the shielding gas flow rate or with the type of gas as shown in Fig. 13. The rates predicted by the model are in fair agreement with the experimental data. Furthermore, the vaporization rates predicted by the Langmuir equation are significantly higher than the corresponding experimental values.

Conclusions

Laser-induced vaporization rates of the various alloying elements predicted from the principles of gas dynamics and weld pool transport phenomena are shown to be in good agreement with the experimental values. Vaporization rates predicted by the Langmuir equation were found to be much higher than the experimental rates. The computed composition of the vapor was in reasonable agreement with the experimentally determined value. The theoretically predicted weld pool geometry and the peak temperature were in good agreement with the corresponding experimentally determined values. Evaporative heat loss was found to significantly decrease the temperature at the pool surface. Independent experimental results on the effect of shielding gas flow rate and the type of shielding gas on the vaporization rate could be explained on the basis of the model for the laser-induced vaporization based on gas dynamics and weld pool transport phenomena.

Acknowledgment

This work was supported by the U.S. Department of Energy, Office of Basic Energy Sciences, Division of Materials Science, under grant number DE-FGO2-84ER45158.

References

1. Khan, P. A. A., DebRoy, T., and David, S. A. 1983. *Welding Journal* 67(1):1-s to 7-s.
2. Khan, P. A. A., and DebRoy, T. 1984. *Metall. Trans. B*, 15B:641–644.
3. Cieslak, M. J., and Fuerschbach, P. W. 1988. *Metall. Trans. B* 19B:319–329.
4. Collur, M. M., Paul, A., and DebRoy, T. 1987. *Metall. Trans. B* 18B:733–740.
5. Miller, R., and DebRoy, T. 1990. *J. App. Phys.* 68(5):2045–2050.
6. Collur, M. M., and DebRoy, T. 1989. *Metall. Trans. B* 20B:277–286.
7. Dunn, G. J., Allemand, C. D., and Eagar, T. W. 1986. *Metall. Trans. A* 17A:1851–1863.
8. Block-Bolten, A., and Eagar, T. W. 1984. *Metall. Trans. B* 15B:461–469.
9. Sahoo, P., Collur, M. M., and DebRoy, T. 1988. *Metall. Trans. B* 19B:967–972.
10. Anisimov, S. I., and Rakhmatulina, A. Kh. 1973. *Soviet Physics-JETP* 37:441–444.
11. Knight, C. J. 1979. *AIAA Journal* 17:519–523.
12. Chan, C. L., and Mazumder, J. 1987. *J. Appl. Phys.* 62:4579–4586.
13. DebRoy, T., Basu, S., and Mundra, K. 1991. *J. Appl. Phys.* 70:1313–1319.
14. Zacharia, T., David, S. A., and Vitek, J. M. 1990. *Metall. Trans. B* 22B:233–241.
15. Khan, P. A. A. 1987. Ph.D. thesis, Department of Materials Science and Engineering, Pennsylvania State University, University Park, Pa.
16. Paul, A., and DebRoy, T. 1988. *Metall. Trans. B* 19B:851–858.
17. Oreper, G. M., and Szekely, J. 1984. *J. Fluid Mech.* 147:53–79.
18. Zacharia, T., Eraslan, A. H., and Aidun, D. K. 1988. *Welding Journal* 67(1):18-s to 27-s.
19. Schlunder, E. U., and Gniclinski, V. 1967. *Chem.-Ing.-Tech.* 39:578–584.
20. Anisimov, S. I., Bonch-Bruevich, A. M., El'yashevich, M. A., Imas, Ya A., Pavlenko, N. A., and Romanvov, G. S. 1967. *Soviet Physics-Technical Physics.* 11:945–952.
21. Dabby, F. W., and Paek, U. 1972. *IEEE Journal of Quantum Electronics* QE-8:106–111.
22. von Allmen, M. 1987. *Laser-Beam Interactions with Materials.* Springer-Verlag, p. 161.
23. Batanov, V. A., Bunkin, F. V., Prokhorov, A. M., and Fedorov, V. B. 1973. *Soviet Physics JETP* 36(2):311–322.
24. Zacharia, T., David, S. A., Vitek, J. M., and DebRoy, T. 1989. *Welding Journal* 68(12):499-s to 509-s.
25. Vincenti, W. and Itrtiger, J. 1965. *Introduction to Physical Gas Dynamics.* Wiley, New York, N.Y.
26. Mehrabian, R., Kou, S., Hsu, S. C., and Munitz, A. 1978. AIP Conference Proceedings, MRS, Boston, Mass.
27. Iida, T., and Guthrie, R. L. 1986. *The Physical Properties of Liquid Metals,* Oxford Science Publications, p. 8.
28. Khan, P. A. A., and DebRoy, T. 1985. *Metall. Trans. B* 16B:853–856.
29. Sahoo, P., DebRoy, T., and McNallan, M. J. 1987. *Metall. Trans. B.* 19B:483–491.
30. Hirschfelder, J. O., Curtiss, C. F., and Bird, R. B. *Molecular Theory of Gases and Liquids,* John Wiley & Sons, Inc., New York, N.Y.
31. Hultergen, R., Desai, P. D., Hawkins, D. T., Gleiser, M., Kelley, K. K., and Wagman, D. D. 1973. *Selected Values of the Thermodynamic Properties of the Elements.* ASM International, Materials Park, Ohio, pp. 6, 7.
32. Honig, R. E., and Kramer, D. A. 1970. *Physicochemical Measurements in Metal Research.* Interscience Publishers, New York, N.Y., vol. 4, pp. 505–517.
33. Turkdogan, E. T. 1980. *Physical Chemistry of High Temperature Technology,* Academic Press, 1980.

Appendix A

List of Symbols

a_i activity of the alloying element i
d diameter of the nozzle
D diffusivity of element i in the shielding gas

f_1 vapor velocity distribution function at the pool surface
f_2 velocity distribution function of the vapor transported toward the weld pool surface
f_3 vapor velocity distribution function at the edge of Knudsen layer
h heat transfer coefficient
ΔH_i enthalpy of vaporization of element i
$J_{c,i}$ vaporization flux of an element i due to concentration gradient
J_h local heat flux from the pool surface
J_i vaporization flux of the element i due to a combination of pressure and concentration gradients
J_p total vaporization flux of all elements due to pressure gradient
$J_{p,i}$ vaporization flux of element i due to pressure gradient
k thermal conductivity of the shielding gas
$K_{g,i}$ mass transfer coefficient of element i
m function of the Mach number given by Equation 9
M Mach number
M_i molecular weight of alloying element i
M_v average molecular weight of vapor
n number of alloying elements
Pr Prandtl number
P_2 pressure across the moving interface between the shielding gas and the vapor
P_g ambient pressure
P_i^o equilibrium vapor pressure of the pure element i
P_1 equilibrium vapor pressure at the pool surface
r radial distance on the pool surface
R gas constant
Re Reynolds number
S speed of sound in vapor
Sc Schmidt number
T_2 temperature across the moving interface between the shielding gas and the vapor
T_{av} average temperature
T_g ambient temperature
T_1 local weld pool surface temperature
T_v temperature at the edge of Knudsen layer
u mean velocity of the vapor at the edge of Knudsen layer

Greek Symbols

ß condensation factor given by Equation 5
ξ velocity of a vapor molecule
γ_g ratio of specific heats at constant pressure and volume for the shielding gas
γ_v ratio of specific heats at constant pressure and volume for the vapor
ρ_2 density across the moving interface between the shielding gas and the vapor
ρ_1 density of the vapor at the pool surface
ρ_v density of the vapor at the edge of Knudsen layer

Appendix B

Calculation of Thermophysical Properties of Gases and Vapor.

The thermal conductivity of shielding gas is given by

$$k_g = \frac{3.9523\times10^{-2}}{\sigma_g^2\Omega_k^*(T^*)}\sqrt{\frac{T}{M_g}} \qquad (1A)$$

where K_g is in J/m-s-k, σ is the collision diameter in angstroms, $T^* = k_B T/\varepsilon$ where k_B is the Boltzmann constant, ε is the intermolecular force parameter, M_g is the molecular weight of the shielding gas and Ω_k is the slowly varying function of the dimensionless parameter kT/ε.

The viscosity of the shielding gas in kg/m-s at temperature T is given by

$$\mu_g = \frac{2.6693\times10^{-6}}{\sigma_g^2\Omega_\mu^*(T^*)}\sqrt{M_g T} \qquad (2A)$$

where Ω_μ is again a slowly varying function of the dimensionless parameter kT/ε.

The mass diffusivity of an element i in the shielding gas, $D_{i,g}$, at absolute temperature T is given by

$$D_{i,g} = \frac{1.8583\times10^{-7}\sqrt{\left(\frac{1}{M_i}+\frac{1}{M_g}\right)T^3}}{\sigma_{i,g}^2\Omega_{D,i}(T^*)} \qquad (3A)$$

where $D_{i,g}$ is in m^2/s, M_i is the molecular weight of the element i, $\sigma_{i,g} = (\sigma_i + \sigma_g)/2$, $\Omega_{D,i}$ is a slowly varying function of $T/\varepsilon_{i,g}$ where

$$\varepsilon_{i,g} = \sqrt{(\varepsilon)_i(\varepsilon)_g} \qquad (4A)$$

The data used for the various parameters are given in Table 6. The values of Ω were obtained from Ref. 30.

Appendix C

Equilibrium Vapor Pressure Data Used for the Calculations

The equilibrium vapor pressures of the various vaporizing species, *viz.*, Mn, Cr, Ni and Fe over the respective pure liquids, at temperature T, expressed in atmospheres were calculated using the following equations:

$\log P^0_{Mn} = -5.58 \times 10^{-4}T - 1.503 \times 10^4/T + 12.609/1.013\times10^5$ (Ref. 31)

$\log P^0_{Ni} = -3.519 \times 10^3/T + 74.94 \log T - 18.042 \times 10^{-3}T + 15.14 \times 10^{-7}T^2 - 214.297/1.013 \times 10^5$ (Ref. 32)

$\log P^0_{Cr} = -13.505 \times 10^3/T + 33.658 \log T - 9.29 \times 10^{-3}T + 8.381 \times 10^{-7}T^2 - 87.077/1.013 \times 10^5$ (Ref. 32)

$\ln P^0_{Fe} = -4.3734 \times 10^4/T + 13.98$ (Ref. 33).

Table 6 — Data Used for the Calculation of the Thermophysical Properties

Parameter	σ (A)	ϵ/k
Iron	2.43	3545.2
Manganese	2.58	2817.9
Chromium	2.46	3738.2
Nickel	2.38	3641.5
Argon	3.418	124.0
Helium	2.576	10.2